
CONTRAST-INVARIANT SELF-SUPERVISED SEGMENTATION FOR QUANTITATIVE PLACENTAL MRI

Xinliu Zhong

Department of Computer Science
Emory University
Atlanta, GA 30307
xinliu.zhong@emory.edu

Ruiying Liu

Department of Biomedical Informatics
Emory University
Atlanta, GA 30307
rliu60@emory.edu

Emily S. Nichols

Department of Pediatrics
Western University
Pomona, CA 91766
enicho4@uwo.ca

Xuzhe Zhang

Department of Biomedical Engineering
Columbia University
New York, NY 10027
xuzhe.z@columbia.edu

Andrew F. Laine

Department of Biomedical Engineering
Columbia University
New York, NY 10027
al418@columbia.edu

Emma G. Duerden

Department of Pediatrics
Western University
Pomona, CA 91766
eduerden@uwo.ca

Yun Wang

Department of Biomedical Informatics
Emory University
Atlanta, GA 30307
yun.wang2@emory.edu

June 13, 2025

ABSTRACT

Accurate placental segmentation is essential for quantitative analysis of the placenta. However, this task is particularly challenging in T2*-weighted placental imaging due to: (1) weak and inconsistent boundary contrast across individual echoes; (2) the absence of manual ground truth annotations for all echo times; and (3) motion artifacts across echoes caused by fetal and maternal movement. In this work, we propose a contrast-augmented segmentation framework that leverages complementary information across multi-echo T2*-weighted MRI to learn robust, contrast-invariant representations. Our method integrates: (i) masked autoencoding (MAE) for self-supervised pretraining on unlabeled multi-echo slices; (ii) masked pseudo-labeling (MPL) for unsupervised domain adaptation across echo times; and (iii) global-local collaboration to align fine-grained features with global anatomical context. We further introduce a semantic matching loss to encourage representation consistency across echoes of the same subject. Experiments on a clinical multi-echo placental MRI dataset demonstrate that our approach generalizes effectively across echo times and outperforms both single-echo and naive fusion baselines. To our knowledge, this is the first work to systematically exploit multi-echo T2*-weighted MRI for placental segmentation.

1 Introduction

The placenta is a vital organ responsible for the exchange of oxygen, nutrients, and waste products between the mother and fetus, playing a central role in supporting fetal development throughout pregnancy [1, 2]. MRI has become increasingly important in placental imaging due to its high soft-tissue contrast, absence of ionizing radiation, multiplanar capabilities, and wide field of view [3]. Compared to ultrasound [4, 5] — the standard modality for prenatal assessment — MRI is less affected by fetal positioning, maternal body habitus, or reduced amniotic fluid, making it a more reliable option in complex or inconclusive cases. These strengths are particularly valuable in diagnosing serious placental

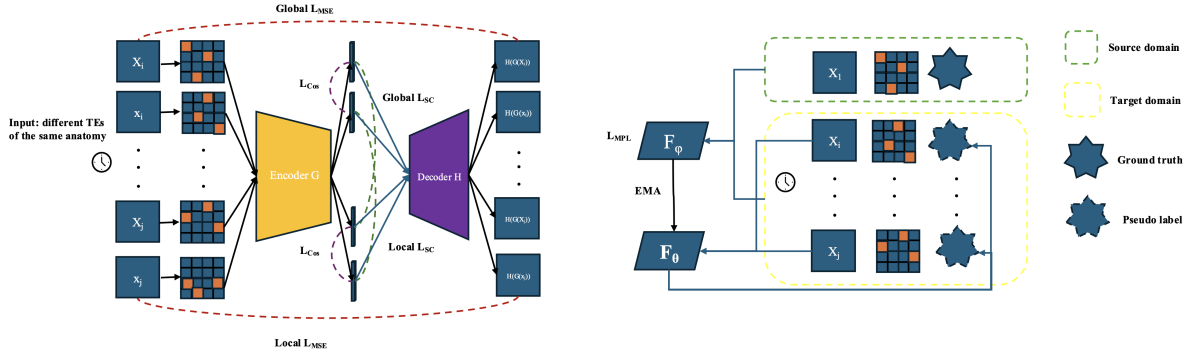
abnormalities such as placenta accreta spectrum (PAS) [6, 7, 8], where abnormal villous invasion into the myometrium can result in severe maternal hemorrhage and life-threatening complications.

In recent years, quantitative MRI techniques such as relaxometry have been developed to evaluate placental function in vivo by capturing signal decay across multiple echo times or time points and generating parametric maps (e.g., T1, T2, T2*) that reflect tissue composition and oxygenation [9, 10]. These quantitative biomarkers offer valuable insights into placental function and development across gestation. However, the reliability of these measurements depends on accurate placental segmentation, which delineates the region of interest for subsequent quantitative analysis.

Several deep learning-based methods have been proposed for placental segmentation, including RFU-Net [11], which utilizes a U-Net architecture; SegNeXt [12], which leverages convolutional neural networks (CNNs); and PLANET-S [13], which combines U-Net and CNN-based components. However, existing work has focused primarily on anatomical imaging, and to date, no studies have addressed segmentation in the context of quantitative MRI data, such as multi-echo T2*-weighted MRI. Segmentation in this setting presents unique challenges. The visual appearance of the placenta can vary substantially across echo times; boundaries that appear well-defined in one echo may become indistinct or disappear entirely in another due to echo-dependent contrast variation. Furthermore, manual ground truth annotations are typically available for only one or a limited subset of echoes, constraining supervised training across the full echo series. In addition, fetal and maternal motion during acquisition can cause misalignment between echoes, introducing spatial inconsistencies that further degrade segmentation performance. Together, these factors hinder the effectiveness of conventional segmentation models and underscore the need for new approaches capable of learning robust, contrast-invariant representations and accommodating motion-induced variability in quantitative placental MRI.

In this work, we revisit multi-echo MRI through the lens of contrast-augmented learning. We hypothesize that contrast variation across echoes can be harnessed as a natural self-supervised signal to facilitate robust, contrast-invariant representation learning. To this end, we propose a segmentation framework that integrates: (i) masked autoencoding for self-supervised pretraining on unlabeled multi-echo data, (ii) pseudo-labeling to enable unsupervised domain adaptation across echo times, and (iii) global-local consistency learning to align fine-grained structural cues with broader anatomical context. Together, these components encourage the model to focus on underlying anatomy rather than echo-specific appearance, yielding improved segmentation generalization across echo times. We validate our method on a clinical multi-echo T2*-weighted placental MRI dataset and compare its performance against conventional supervised baselines, including MONAI-fbs [14].

2 Methods



(a) MAE Pretraining. Multi-echo slices are masked and encoded using a shared encoder. The model is trained with reconstruction loss (\mathcal{L}_{MSE}), semantic consistency loss (\mathcal{L}_{SC}), and global local collaboration loss (\mathcal{L}_{Cos}) across local/global views.

(b) MPL Training. A teacher-student segmentation setup leverages pseudo labels for unlabeled target slices. The teacher F_θ is updated by EMA, and the student F_ϕ is optimized using the MPL loss \mathcal{L}_{MPL} .

Figure 1: Overview of our two-stage training framework. (a) Semantic masked autoencoding encourages robust contrast-invariant representations across echo times. (b) Masked pseudo-labeling enables segmentation adaptation using cross-domain pseudo supervision.

We propose a segmentation framework that maps multi-echo T2*-weighted placental images x_{TE_i} (where $TE_i = 1, \dots, n$ indexes number of echo times) to corresponding segmentation masks y_i . Our design addresses the unique

challenges of fetal MRI—such as motion artifacts, inter-echo contrast variation, and sparse supervision—through four integrated components:

2.1 2D Masked Autoencoding

To learn contrast-invariant anatomical representations without supervision, we adopt a 2D masked autoencoder (MAE [15, 16]). Each input slice is processed in two complementary forms: a local image patch x and its corresponding globally downsampled slice X . Before being passed to the encoder, both are partially masked to produce x^M and X^M , respectively.

The model is trained to reconstruct the original x and X from their masked versions, using a reconstruction loss over the missing regions:

$$\mathcal{L}_{\text{MAE}} = \text{MSE}(g(x^M), x) + \text{MSE}(g(X^M), X),$$

where $g(\cdot)$ is the shared MAE encoder-decoder pipeline. This dual-scale training encourages the model to integrate fine-grained and global spatial cues, enabling robust pretraining across contrast-varying inputs.

2.2 2D Pseudo-Labeling

To enable unsupervised domain adaptation across echo times, we extend the masked pseudo-labeling (MPL [15]) framework to a 2D setting. After pretraining, the MAE encoder g is retained, and a segmentation decoder h is added to form the segmentation model $f = h \circ g$.

We consider a labeled source domain slice x_s with its annotation y_s , and an unlabeled target domain slice x_t . Both undergo the same masking strategy used in pretraining, yielding x_s^M and x_t^M . A teacher model f_θ (with parameters θ) predicts a pseudo-label $\hat{y}_t = f_\theta(x_t)$ for the target image. The student model f_ϕ is trained with a hybrid objective:

$$\mathcal{L}_{\text{MPL}} = \mathcal{L}_{\text{Seg}}(f_\phi(x_t^M), \hat{y}_t) + \beta \mathcal{L}_{\text{Seg}}(f_\phi(x_s^M), y_s),$$

where β controls the source-vs-target supervision ratio, and \mathcal{L}_{Seg} denotes a segmentation loss function (e.g., Dice or cross-entropy). The teacher parameters are updated using exponential moving average (EMA):

$$\theta_{t+1} \leftarrow \alpha \theta_t + (1 - \alpha) \phi_t.$$

This framework enables learning from unlabeled echoes by guiding the model with stable predictions, while still anchored to supervised TE1 annotations.

2.3 Global-Local Collaboration

To further improve segmentation robustness under domain shifts, we introduce a global-local collaboration (GLC [15]) module that fuses anatomical cues from different spatial scales. Given a local patch x and the downsampled slice X , the encoder produces latent features $\chi_{\text{loc}} = g(x)$ and $\chi_{\text{glo}} = \text{upsample}(M \odot g(X))$, where M denotes the location of x within X and \odot is a cropping operation.

These two features are concatenated and passed to the decoder:

$$f(x) = h(\chi_{\text{loc}} \oplus \chi_{\text{glo}}),$$

where \oplus denotes channel-wise concatenation. An auxiliary branch is also trained on X alone to discourage overreliance on local features. We further regularize similarity between χ_{loc} and χ_{glo} via cosine similarity:

$$\mathcal{L}_{\text{cos}}(x, X) = 1 - \frac{\chi_{\text{loc}} \cdot \chi_{\text{glo}}}{\max(\|\chi_{\text{loc}}\|_2, \|\chi_{\text{glo}}\|_2, \epsilon)}.$$

This encourages the encoder to align local and global representations for consistent decoding, even under spatial or contrast shifts.

2.4 Semantic Matching

To promote consistency in latent representations across different echo times (TEs), we employ a semantic matching module that combines both contrast-invariant feature alignment and soft target distillation. This design is motivated by the observation that different echoes of the same anatomical slice should yield semantically consistent features, even under varied image contrasts.

MAE Stage. During masked autoencoding, paired slices (x_i, x_j) from the same spatial location but different TEs are passed through a shared encoder and decoder to produce features $t_i^{\text{enc}}, t_j^{\text{enc}}, t_i^{\text{dec}}, t_j^{\text{dec}}$. We define the semantic consistency loss as:

$$\mathcal{L}_{\text{SC}}^{\text{MAE}} = \lambda_{\text{enc}}(1 - \cos(t_i^{\text{enc}}, t_j^{\text{enc}})) + \lambda_{\text{dec}}(1 - \cos(t_i^{\text{dec}}, t_j^{\text{dec}})), \quad (1)$$

where $\cos(\cdot, \cdot)$ denotes cosine similarity.

MPL Stage. After MAE pretraining, we train a segmentation model using a teacher-student MPL framework. We continue applying semantic matching to the student’s encoder and decoder features using echo or augmented pairs:

$$\mathcal{L}_{\text{SC}}^{\text{MPL}} = \lambda'_{\text{enc}}(1 - \cos(t_i^{\text{enc}}, t_j^{\text{enc}})) + \lambda'_{\text{dec}}(1 - \cos(t_i^{\text{dec}}, t_j^{\text{dec}})). \quad (2)$$

While knowledge distillation is standard in teacher-student learning, we omit KL-divergence losses [17] from our semantic consistent module for three reasons: (1) hard pseudo-labels from the teacher already provide strong supervision; (2) both teacher and student share identical architectures, reducing the benefit of soft-logit matching; and (3) cosine loss offers a simpler and more stable alignment objective.

3 Materials and Experiments

3.1 Dataset

Placental multi-echo T2*-weighted MR images were collected from a prospective cohort of pregnant individuals at Western University between December 2020 and August 2023. All scans were acquired in the coronal orientation using customized 2D pulse sequences with 16 echo times (TEs) ranging from 3.15 ms to 77.31 ms and a fixed repetition time (TR) of 81.1 ms. Each echo captured the same anatomical slice with varying contrast, offering complementary tissue-specific information. Slice thickness was 5 mm, and signal intensity varied across TEs due to tissue relaxation dynamics.

Patient Selection and Enrollment A total of 54 participants were enrolled, each undergoing one or two MRI sessions during the third trimester (\geq two weeks apart). Session 1 included 53 participants, and 44 returned for Session 2. Mean gestational ages were 31.8 weeks (Session 1) and 34.1 weeks (Session 2). The cohort comprised 22 female (40.7%), 30 male (55.6%), and 2 unknown-sex fetuses. Maternal age averaged 31.9 years (range: 22–41), and socioeconomic status was 29.1 (SD = 12.0) on a 0–45 scale.

MRI Equipment and Parameters Imaging was performed on a 3T GE Discovery MRI scanner using a 32-channel torso coil. Anatomical sequences were also acquired in axial, coronal, and sagittal planes using single-shot fast spin-echo protocols (TR > 1,000 ms, TE = 80 ms, 19–25 slices). In-plane resolution was 0.74×0.74 mm (coronal/sagittal) or 0.86×0.86 mm (axial), with a field of view (FOV) of 38–44 mm. Preprocessing included motion correction, bias field correction, and super-resolution reconstruction to 1 mm isotropic resolution. Each subject’s data was nonlinearly registered to a 36-week gestational age fetal brain atlas [18], with atlas-based labels warped to native space.

Image Selection and Annotation From each eligible scan, a senior radiologist manually selected two consecutive slices in which the placenta was clearly visible. This yielded a total of 209 annotated 2D multi-echo sequences (each with 16 echo times) across the 54 patients. Manual segmentation of the placental region was performed using FSLeaves version 1.6.1 (FMRIB Software Library), and annotations were visually reviewed to ensure anatomical accuracy.

3.2 Data Splitting Strategy

To study contrast-invariant representation learning across TEs, we devised a partitioning strategy that isolates data used for masked autoencoding (MAE) pretraining from those used for pseudo-label-based domain adaptation (MPL).

We designate TE1 as the labeled source domain and treat all other echo times as part of a shared pool (TE_{other}) for unlabeled target domains. The data splitting proceeds as follows:

MAE Pretraining Subset Ten TEs are randomly sampled from TE_other , each contributing 105 slices, forming an unsupervised pretraining dataset of 10×105 slices. This subset is used exclusively for masked autoencoding and remains disjoint from downstream segmentation tasks.

MPL Domain Adaptation For the source domain, we use 10×100 labeled slices from TE1, each paired with a manual segmentation mask. For the target domain, we randomly select 5 different TEs from TE_other (non-overlapping with the MAE set), contributing 5×105 unlabeled slices. These are used in the MPL setup to simulate domain shifts in contrast and assess adaptation robustness.

To further investigate model robustness under varying levels of contrast discrepancy, we define three specific target domain settings using TE6, TE10, and a grouped domain composed of TEs 14, 15, and 16. Each scenario provides a distinct challenge in terms of echo characteristics and serves to benchmark generalization performance across different contrast shifts.

Validation Protocol For validation, we randomly reserve five subjects from the source-domain training pool, yielding 18 labeled TE1 slices. These are held fixed across all experimental runs for consistent comparison. Importantly, all data splits are performed at the subject level to ensure no patient overlap between training, validation, or evaluation sets, thus avoiding potential leakage and ensuring reliable performance evaluation.

3.3 Model Training and Testing

We trained the model in two sequential stages: (1) masked autoencoding (MAE) for self-supervised representation learning, and (2) masked pseudo-labeling (MPL) for supervised and unsupervised domain adaptation.

MAE Pretraining. Self-supervised pretraining was performed on unlabeled multi-echo slices. We used a 2D convolutional encoder-decoder architecture with 8 layers and an embedding dimension of 512. Inputs included both a local patch x and a globally downsampled image X , each resized to 256×256 pixels. For masking, x was divided into non-overlapping 8×8 patches, and X into 4×4 patches. In both cases, 70% of patches were randomly masked to generate x_M and X_M . The decoder was trained to reconstruct the unmasked input from these masked versions by minimizing the mean squared error (MSE) on masked regions: $\mathcal{L}_{MAE} = \text{MSE}(g(x_M), x) + \text{MSE}(g(X_M), X)$.

To encourage contrast-invariant representations, we applied semantic consistency loss across echo pairs. Let $t_i^{\text{enc}}, t_j^{\text{enc}}$ and $t_i^{\text{dec}}, t_j^{\text{dec}}$ denote the encoder and decoder features for paired slices (x_i, x_j) :

$$\mathcal{L}_{SC}^{\text{MAE}} = \lambda_{\text{enc}}(1 - \cos(t_i^{\text{enc}}, t_j^{\text{enc}})) + \lambda_{\text{dec}}(1 - \cos(t_i^{\text{dec}}, t_j^{\text{dec}})).$$

The total MAE objective is:

$$\mathcal{L}_{MAE\text{-total}} = \mathcal{L}_{\text{MSE}} + \gamma_{SC}^{\text{MAE}} \cdot \mathcal{L}_{SC}^{\text{MAE}}.$$

Training was performed for 300 epochs with a constant learning rate of 2×10^{-4} , using the AdamW optimizer (weight decay = 0.05, $\beta_1 = 0.9$, $\beta_2 = 0.95$) and a batch size of 4.

MPL Pseudo-Labeling Training. Following MAE pretraining, the segmentation network $f = h \circ g$ was initialized with the pretrained encoder g , and a segmentation decoder h was attached. For each batch, one labeled TE1 slice x_s with ground truth y_s , and one unlabeled target echo x_t were processed. Both inputs were masked using the same patch strategy from MAE, resulting in x_s^M and x_t^M . The pseudo-label $\hat{y}_t = f_\theta(x_t)$ was generated by an EMA-updated teacher model f_θ . The student model f_ϕ was trained to minimize: $\mathcal{L}_{MPL} = \mathcal{L}_{\text{Seg}}(f_\phi(x_t^M), \hat{y}_t) + \beta \mathcal{L}_{\text{Seg}}(f_\phi(x_s^M), y_s)$, where $\beta = 0.5$, and \mathcal{L}_{Seg} is a combination of Dice and cross-entropy loss. EMA parameters were updated as: $\theta_t + 1 = \alpha \theta_t + (1 - \alpha) \phi_t$, with an adaptive decay schedule: $\alpha = 0.99$ (first 1k steps), $\alpha = 0.999$ (next 2k), and $\alpha = 0.9999$ thereafter.

To maintain semantic alignment during segmentation, we applied the same consistency loss as in MAE to student features:

$$\mathcal{L}_{SC}^{\text{MPL}} = \lambda'_{\text{enc}}(1 - \cos(t_i^{\text{enc}}, t_j^{\text{enc}})) + \lambda'_{\text{dec}}(1 - \cos(t_i^{\text{dec}}, t_j^{\text{dec}})).$$

The total MPL training loss becomes:

$$\mathcal{L}_{MPL\text{-total}} = \mathcal{L}_{MPL} + \gamma_{SC}^{\text{MPL}} \cdot \mathcal{L}_{SC}^{\text{MPL}}.$$

Training ran for 150 epochs with a warmup of 50 epochs. We used AdamW with learning rate 1×10^{-4} , weight decay 0.01, $\beta_1 = 0.9$, $\beta_2 = 0.999$, batch size = 1, and early stopping patience = 75 epochs.

Data Handling. Input images were normalized to the 99.5th percentile and background regions were removed. Data augmentation included random horizontal/vertical flips and intensity jittering, applied with a 0.35 probability.

Training Infrastructure. All models were implemented in PyTorch and trained on NVIDIA H100 GPUs. Checkpoints were saved every 50 epochs. Training progress and visualizations were tracked using Weights & Biases (wandb). The segmentation model used in both MAE and MPL phases shares the same encoder, promoting stable feature reuse.

4 Results and Discussion

4.1 Results

4.1.1 Quantitative Performance

Table 1 summarizes the segmentation accuracy achieved by different training strategies using the Dice coefficient. The Dice score measures the overlap between the predicted placental pixels and the ground-truth placental region, defined as:

$$\text{Dice} = \frac{2 \cdot TP}{2 \cdot TP + FP + FN}, \quad (3)$$

where TP (True Positive) and TN (True Negative) represent the number of pixels correctly predicted as placenta and background, respectively. FP (False Positive) indicates background pixels incorrectly labeled as placenta, while FN (False Negative) denotes placental pixels missed by the model. A Dice score closer to 1 indicates higher segmentation accuracy.

Table 1: Segmentation performance (Dice coefficient %) across different training setups.

Model	Dice (%)	Description
Proposed	91.8	Ours with full two-stage pipeline
Ours (w/o domain split)	91.2	Same pipeline without domain-specific pairing
MONAIfbs baseline [14]	79.95	Public SOTA method without pretraining

Even without explicit domain pairing, our model still achieves a strong Dice score of 91.2%, highlighting the robustness of the learned features. In contrast, MONAIfbs—trained directly on source-labeled data—underperforms significantly at 79.95%, likely due to its limited capacity to generalize across varying echo contrasts.

4.1.2 Qualitative Analysis

Figure 2 illustrates sample reconstructions during MAE pretraining. The model effectively reconstructs masked regions in both local patches and global views, indicating successful encoding of structural and contextual information. This dual-scale consistency is foundational for downstream segmentation.

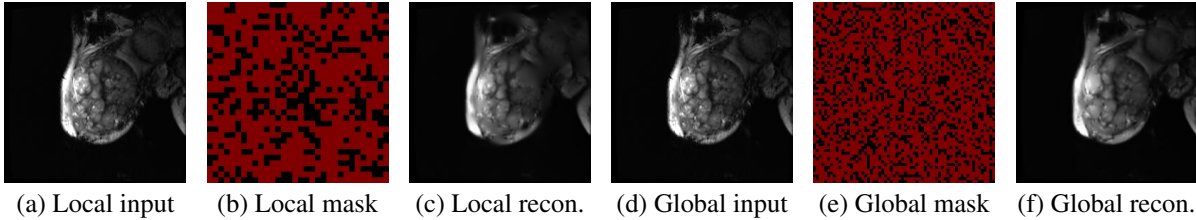


Figure 2: Qualitative results from MAE pretraining. (a–c) show masked reconstruction for a local patch: original, mask, and prediction. (d–f) show the same for the downsampled global slice. The dual-scale design encourages the model to capture both local structures and broader anatomical context.

In Figure 3, we visualize source and target domain predictions. In the source domain, predictions closely match ground truth. In the target domain, the student model accurately segments anatomical structures based on pseudo-labels, indicating strong domain adaptation. Notably, boundary consistency is preserved, even for faint echo contrasts.

4.2 Discussion

The observed performance gains validate the effectiveness of our two-stage framework. MAE pretraining provides a strong initialization, enabling the encoder to learn echo-invariant anatomical representations. Subsequent MPL training fine-tunes these features toward segmentation with limited supervision.

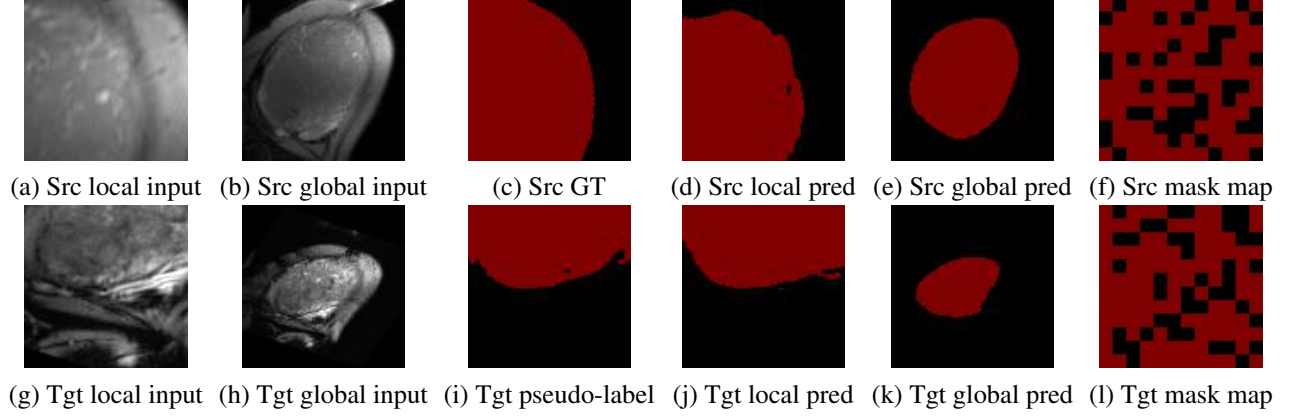


Figure 3: Qualitative results of segmentation and pseudo-labeling. Top row (a–f): source domain inputs with ground truth annotations and predictions. Bottom row (g–l): target domain inputs with pseudo-labels and predicted segmentations.

Interestingly, the performance drop (91.8% to 91.2%) without domain-aware pairing suggests that paired echo supervision contributes marginal but consistent benefits. However, the model still performs robustly in its absence, indicating generalizability.

In contrast, MONAIfbs suffers from lower Dice scores, demonstrating that without pretraining or adaptation, traditional models fail to bridge domain gaps caused by multi-echo contrast variation.

Overall, the proposed method offers a lightweight yet effective alternative to heavy 3D architectures, with particular strength in cross-contrast generalization and low-data regimes.

5 Conclusion

We presented a two-stage segmentation framework for multi-echo placental MRI, combining self-supervised pretraining via masked autoencoding (MAE) with semi-supervised domain adaptation using masked pseudo-labeling (MPL). The MAE module enables the encoder to learn contrast-invariant representations from unlabeled multi-echo slices, while the MPL stage leverages a teacher-student architecture to adapt the segmentation model across echo time variations using both labeled and unlabeled data.

Through experiments on challenging multi-echo datasets, our method achieved a Dice score of 91.8%, significantly outperforming both a non-adaptive baseline (91.2%) and a recent domain adaptation approach (MONAIfbs: 79.95%). Qualitative results further demonstrate our model’s ability to generalize across echo contrasts and anatomical variability.

Our findings highlight the importance of integrating self-supervised representation learning with targeted adaptation strategies for robust medical image segmentation. Future work will explore extending the framework to 3D volumes and applying it to other contrast-shifted imaging modalities.

References

- [1] TRH Regnault, HL Galan, TA Parker, and RV Anthony. Placental development in normal and compromised pregnancies—a review. *Placenta*, 23:S119–S129, 2002.
- [2] Alan E Guttmacher, Yvonne T Maddox, and Catherine Y Spong. The human placenta project: placental structure, development, and function in real time. *Placenta*, 35(5):303–304, 2014.
- [3] E Routledge, C Malamateniou, and M Rutherford. Can mr imaging of the placenta demonstrate a distinct placental phenotype in normal and abnormal pregnancies. *Bachelor Sci. Degree Imag. Sci., King’s College London, Univ. London, London, UK, Tech. Rep*, 2015.
- [4] Ümmü Özkaya, Sebiha Özkan, Semih Özeren, and Aydın Çorakçı. Doppler examination of uteroplacental circulation in early pregnancy: can it predict adverse outcome? *Journal of Clinical Ultrasound*, 35(7):382–386, 2007.

- [5] Leona C Poon, Cristina Lesmes, Dahiana M Gallo, Ranjit Akolekar, and Kypros H Nicolaides. Prediction of small-for-gestational-age neonates: screening by biophysical and biochemical markers at 19–24 weeks. *Ultrasound in obstetrics & gynecology*, 46(4):437–445, 2015.
- [6] Whitney Booker and Leslie Moroz. Abnormal placentation. In *Seminars in perinatology*, volume 43, pages 51–59. Elsevier, 2019.
- [7] Jennifer L Bailit, William A Grobman, Madeline Murguia Rice, Uma M Reddy, Ronald J Wapner, Michael W Varner, Kenneth J Leveno, Jay D Iams, Alan TN Tita, George Saade, et al. Morbidly adherent placenta treatments and outcomes. *Obstetrics & Gynecology*, 125(3):683–689, 2015.
- [8] Eric Jauniaux, Catey Bunce, Lene Grønbeck, and Jens Langhoff-Roos. Prevalence and main outcomes of placenta accreta spectrum: a systematic review and meta-analysis. *American journal of obstetrics and gynecology*, 221(3):208–218, 2019.
- [9] E Mark Haacke, Saifeng Liu, Sagar Buch, Weili Zheng, Dongmei Wu, and Yongquan Ye. Quantitative susceptibility mapping: current status and future directions. *Magnetic resonance imaging*, 33(1):1–25, 2015.
- [10] Zungho Zun, Kushal Kapse, Jessica Quistorff, Nickie Andescavage, Alexis C Gimovsky, Homa Ahmadzia, and Catherine Limperopoulos. Feasibility of qsm in the human placenta. *Magnetic Resonance in Medicine*, 85(3):1272–1281, 2021.
- [11] Jun Li, Zhijie Shi, Jialiang Zhu, Jin Liu, Lihua Qiu, Yeye Song, Liquan Wang, Yuling Li, Yongliang Liu, Dawei Zhang, et al. Placenta segmentation in magnetic resonance imaging: Addressing position and shape of uncertainty and blurred placenta boundary. *Biomedical Signal Processing and Control*, 88:105680, 2024.
- [12] Meng-Hao Guo, Cheng-Ze Lu, Qibin Hou, Zhengning Liu, Ming-Ming Cheng, and Shi-Min Hu. Segnext: Rethinking convolutional attention design for semantic segmentation. *Advances in neural information processing systems*, 35:1140–1156, 2022.
- [13] Shinnosuke Yamamoto, Issa Saito, Eichi Takaya, Ayaka Harigai, Tomomi Sato, Tomoya Kobayashi, Kei Takase, and Takuya Ueda. Planet-s: Automatic semantic segmentation of placenta. *arXiv preprint arXiv:2312.11580*, 2023.
- [14] Marta Ranzini, Lucas Fidon, Sébastien Ourselin, Marc Modat, and Tom Vercauteren. Monai-fbs: Monai-based fetal brain mri deep learning segmentation. *arXiv preprint arXiv:2103.13314*, 2021.
- [15] Xuzhe Zhang, Yuhao Wu, Elsa Angelini, Ang Li, Jia Guo, Jerod M Rasmussen, Thomas G O’Connor, Pathik D Wadhwa, Andrea Parolin Jackowski, Hai Li, et al. Mapseg: Unified unsupervised domain adaptation for heterogeneous medical image segmentation based on 3d masked autoencoding and pseudo-labeling. In *Proceedings of the IEEE/CVF Conference on Computer Vision and Pattern Recognition*, pages 5851–5862, 2024.
- [16] Kaiming He, Xinlei Chen, Saining Xie, Yanghao Li, Piotr Dollár, and Ross Girshick. Masked autoencoders are scalable vision learners. In *Proceedings of the IEEE/CVF conference on computer vision and pattern recognition*, pages 16000–16009, 2022.
- [17] Yimu Pan, Sitao Zhang, Alison D Gernand, Jeffery A Goldstein, and James Z Wang. S2s2: Semantic stacking for robust semantic segmentation in medical imaging. In *Proceedings of the AAAI Conference on Artificial Intelligence*, volume 39, pages 6335–6344, 2025.
- [18] Ali Gholipour, Caitlin K Rollins, Clemente Velasco-Annis, Abdelhakim Ouaham, Alireza Akhondi-Asl, Onur Afacan, Cynthia M Ortinau, Sean Clancy, Catherine Limperopoulos, Edward Yang, et al. A normative spatiotemporal mri atlas of the fetal brain for automatic segmentation and analysis of early brain growth. *Scientific reports*, 7(1):476, 2017.